Journal of Power Sources 196 (2011) 2109–2114

Contents lists available at ScienceDirect

Journal of Power Sources

journal homepage: www.elsevier.com/locate/jpowsour

A comparative study on the low-temperature performance of $LiFePO_4$/C and $Li_3V_2(PO_4)_3$/C cathodes for lithium-ion batteries

X.H. Rui, Y. Jin, X.Y. Feng, L.C. Zhang, C.H. Chen*

CAS Key Laboratory of Materials for Energy Conversion, Department of Materials Science and Engineering, University of Science and Technology of China, Anhui, Hefei 230026, China

ARTICLE INFO

Article history:
Received 24 July 2010
Received in revised form
24 September 2010
Accepted 21 October 2010
Available online 30 October 2010

Keywords:
Lithium iron phosphates
Lithium vanadium phosphates
Carbon coating
Diffusion coefficient
Activation energy

ABSTRACT

The electrochemical properties of the $LiFePO_4$/C (LFP/C) and $Li_3V_2(PO_4)_3$/C (LVP/C) samples are investigated using Li-ion half cells at various low temperatures of 23, 0, −10 and −20 °C in the electrolyte 1.0 M $LiPF_6$/EC + DMC (1:1 w/w). In the voltage range of 2.5–4.3 V at 0.3 C rate, the LFP/C electrode shows a stable reversible discharge capacity of 45.4 mAh g^{-1} at −20 °C, which is 31.5% of the capacity obtained at 23 °C. In the voltage range of 3.0–4.3 V at 0.3 C rate, the LVP/C electrode delivers a high stable reversible discharge capacity of 108.1 mAh g^{-1} at −20 °C, being 86.7% of the capacity at 23 °C. The electrochemical impedance spectroscopy (EIS) and cyclic voltammetry (CV) measurements illustrate that the resistance and cell polarization of LFP/C at various low temperatures are larger than those of LVP/C. In addition, using CV method, the apparent chemical diffusion coefficient of lithium ions ($D^{app}_{Li^+}$) in LFP and LVP at various low temperatures are in the magnitude of 10^{-11} and 10^{-10} cm^2 s^{-1}, respectively, and the $D^{app}_{Li^+}$ decreasing rate of LFP as the temperature is much larger than LVP, meaning that the kinetics of the LFP electrode is relatively slow. The activation energies of LFP and LVP are calculated to be 47.48 and 6.57 kJ mol^{-1}, respectively, which further indicates that the extraction/intercalation of Li^+ in LVP is much easier than in LFP. The high reversible capacity of LVP/C at −20 °C makes it an attractive cathode for low-temperature lithium ion batteries.

1. Introduction

Rechargeable lithium-ion batteries (LIBs) have become very important components in electronic devices as well as in electric vehicles (EVs) and hybrid electric vehicles (HEVs). $LiCoO_2$ is the currently widely applied cathode material in commercial lithium-ion batteries owing to its relatively good electrochemical properties and the convenience of preparation. However, it suffers from high cost, toxicity and inferior safety [1,2]. Recently, NASICON or olivine polyoxyanion structures, built from MO_6 octahedra (where M is Fe, Co, Mn, Ni, V or Ti) and XO_4^{n-} (where X is P, W, S or Mo) tetrahedral anions, have been discovered as cathode materials with high safety [3–8].

Since the olivine-type $LiFePO_4$ (LFP) was first reported by Padhi et al. [2] in 1997, it holds great promises as the possible substitute for $LiCoO_2$ for electric vehicles applications. It is because that LFP possess high theoretical capacity (170 mAh g^{-1}), inexpensiveness, natural abundance, environmental friendliness, thermal stability in the fully charged state and good cycle stability [9,10]. The main feature of the $LiFePO_4$ crystal structure consists of olivine-type ribbons extending along the b crystal axis. The Li^+ insertion/extraction into $LiFePO_4$ is in a two-phase mechanism. One Li^+ can be reversibly removed from it, leading to a crystalline form of the composition $FePO_4$, which retains the olivine-type structure with a volume decrease of only 6.81% and density increase of 2.59% compared to LFP [2]. Such characteristics ensure an excellent cycling stability. On the other hand, the monoclinic $Li_3V_2(PO_4)_3$ (LVP) has also recently attracted considerable interest as the cathode material [6]. Except for competitive energy density and good thermal stability, it is also demonstrated to have outstanding electrochemical performance with good ionic mobility, high reversible capacity and relatively high operating voltage [6,11]. The monoclinic LVP structure consists of a 3D framework of slightly distorted VO_6 octahedra and PO_4 tetrahedra sharing oxygen vertexes [6,12–14]. Such framework containing corner-shared chains of Li polyhedra and interconnected interstitial space is potentially a fast ionic conductor. It can extract and insert two lithium ions reversibly between 3.0 and 4.3 V based on the V^{3+}/V^{4+} redox couple, corresponding to a theoretical capacity of 133 mAh g^{-1}. In this voltage range, the charge–discharge mechanisms of LVP are three consecutive two-phase transition processes, occurring at 3.65 V ($Li_3V_2(PO_4)_3 \leftrightarrow Li_{2.5}V_2(PO_4)_3$), 3.70 V ($Li_{2.5}V_2(PO_4)_3 \leftrightarrow Li_2V_2(PO_4)_3$) and 4.10 V ($Li_2V_2(PO_4)_3 \leftrightarrow LiV_2(PO_4)_3$).

* Corresponding author. Tel.: +86 551 3606971; fax: +86 551 3601592.
E-mail address: cchchen@ustc.edu.cn (C.H. Chen).

0378-7753/$ – see front matter © 2010 Elsevier B.V. All rights reserved.
doi:10.1016/j.jpowsour.2010.10.063

However, a main drawback of $LiFePO_4$ and $Li_3V_2(PO_4)_3$ is their low intrinsic electronic conductivity (LFP: about 10^{-9} S cm^{-1} [15], LVP: about 10^{-8} S cm^{-1} [14]), which limits their application in high-power-density batteries. Various synthesis and processing approaches have been employed to overcome this problem, which include selective doping with metal cations [16–18] and using carbon-coating strategy [9,19–21]. It is confirmed that the introduction of conductive carbon in LFP and LVP cathodes can effectively promote electronic conductivity and particle connection. The carbon coating is usually realized by introducing an organic precursor in the starting materials. The organic precursors can be converted into electronically conductive carbon through pyrolysis processes at high temperatures under inert atmospheres. In fact, in the synthesis of the carbon coated $Li_3V_2(PO_4)_3$ (LVP/C) composites, the carbon should not only improve electronic conductivity but also act as a reductant to reduce V^{5+} to V^{3+} when a pentavalent vanadium precursor such as NH_4VO_3 is used.

It is known that $LiFePO_4$ and $Li_3V_2(PO_4)_3$ are the very promising cathode materials for large-scale lithium ion batteries, and much attention has been given to improve their basic electrochemical behavior at ambient and high temperatures [21–23]. Nevertheless, many high technology applications, such as military and aerospace missions, require Li-ion batteries to be capable of operating at low-temperatures (e.g. −20 °C or even lower) with appropriate energy density and power capability. Thus, it is very valuable to evaluate their low-temperature performance. Herein, a comparative study of the electrochemical properties of the carbon coated $LiFePO_4$ (LFP/C) and LVP/C cathodes in a general electrolyte (1.0 M $LiPF_6$/EC + DMC (1:1 w/w)) at various low temperatures (23, 0, −10 and −20 °C) was conducted. The electrochemical impedance spectroscopy (EIS) and cyclic voltammetry (CV) were used to determine the performance limiting aspects at low-temperature.

2. Experimental

A LFP/C powder was provided by Lithing Co. Ltd. (Nanjing, China), and it was prepared by a solid state reaction method at 700 °C. Meanwhile, a LVP/C composite powder was also prepared by a solid state reaction method using crystal sugar as the reducing agent as well as carbon source. During the LVP/C synthesis, stoichiometric amounts of Li_2CO_3, V_2O_5 and $NH_4H_2PO_4$ (Li:V:P = 3:2:3) and 40 wt% crystal sugar were dispersed into acetone and then ball milled for two days. The obtained mixtures were dried in an oven at 70 °C to evaporate acetone. Then they were preheated at 350 °C in N_2 atmosphere for 5 h to expel H_2O and NH_3. After that, the precursors were reground and sintered at 750 °C for 16 h under flowing N_2 to yield the LVP/C composites. The amount of carbon in LFP/C sample was about 2.2 wt% measured by dissolving LFP/C in hydrochloric acid solution (36 wt%) and weighing the remains. The residual carbon content in the LVP/C composites is calculated as about 12.0 wt%. The methodology of this residual carbon measurement has been described elsewhere [24].

Structural analyses of LFP/C and LVP/C were performed by the X-ray diffraction (XRD) using a rotating anode X-ray diffractometer (MXPAHF, Cu Kα radiation). The diffraction patterns were recorded at room temperature in the 2θ range from 10° to 60°. The particle morphology of the samples was observed under a scanning electron microscope (SEM, JSM-6390LA). The particle size distribution of the samples was determined by a laser particle sizer (Rise-2008).

The electrochemical tests of LFP/C and LVP/C composites were carried out in coin-type cells. The working electrodes were prepared by mixing 80 wt% active materials, 10 wt% acetylene black and 10 wt% polyvinylidene fluoride (PVDF) in NMP, and then followed by coating the slurry onto Al foil current collector and drying at 70 °C. The lithium metal foil was used as the anode while the electrolyte was a solution of 1 M $LiPF_6$ in a 1:1 (w/w) mixture of EC and DMC. The coin-cells (CR2032 size) were assembled in an argon-filled glove box and tested on a multi-channel battery test system (NEWARE BTS-610) with galvanostatic charge and discharge in the voltage range of 2.5–4.3 V for LFP/C and 3.0–4.3 V for LVP/C under a constant current density of 0.3 C at various low temperatures (23, 0, −10 and −20 °C). Here, it is noted that the cycling at −10 and 0 °C was conducted in a household refrigerator with about ± 4 °C fluctuation. And other electrochemical tests at low temperatures of 0, −10 and −20 °C were performed in a low-temperature test case with almost no temperature fluctuation. In addition, it should be pointed out that the specific capacity data in this paper are based on the mass of the bare LFP and LVP without the residual carbon. Moreover, their cyclic voltammetry and electrochemical impedance spectroscopy (frequency range: 0.001–10^5 Hz) measurements were performed on a CHI 604B electrochemical workstation.

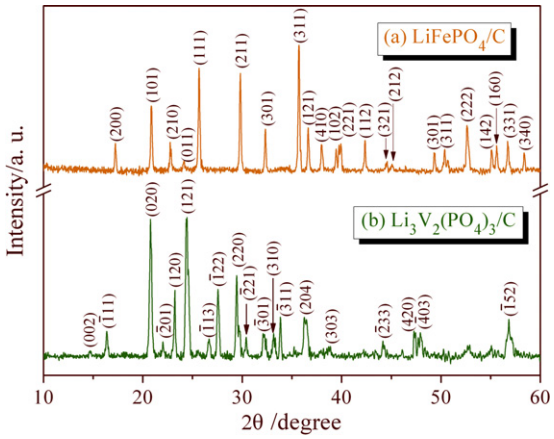

Fig. 1. X-ray diffraction patterns of the LFP/C (a) and LVP/C (b) samples.

3. Results and discussion

The X-ray diffraction patterns (XRD) of LFP/C and LVP/C samples are shown in Fig. 1. All diffraction peaks in Fig. 1a can be indexed as $LiFePO_4$ phase with an ordered orthorhombic olivine structure (space group: *Pnma*). No impurities such as Fe_2P, Li_3PO_4 and others are observed. In addition, all diffraction peaks are narrow, indicating that the LFP gains are with high crystallinity. As shown in Fig. 1b, the diffraction lines can be attributed to a well-crystallized monoclinic $Li_3V_2(PO_4)_3$ phase with the space group of $P2_1/n$. No traces of possible phases such as Li_2O, Li_3PO_4 and Li_3VO_4 were detected. On the other hand, no diffraction peaks corresponding to the carbon present in LFP/C and LVP/C samples are observed, which indicates that the residual carbon is amorphous and/or the thickness of the residual carbon on the LFP and LVP particles is too thin [25,26], and its presence does not influence the structure of LFP and LVP. Furthermore, the grain size (D) is calculated with the Scherrer's equation: $D = 0.9\lambda/(\beta \cos\theta)$, where λ is the X-ray wavelength and β is the full-width-at-half-maximum of the diffraction peak on a 2θ scale. Based on diffraction planes of (3 1 1), (1 1 1) and (2 1 1), the mean value of grain size of LFP ($\bar{D}_{LFP}$) is 50 nm. Meanwhile, ($\bar{D}_{LVP}$) of LVP was calculated to be 42 nm according to diffraction planes of (1 2 1), (0 2 0) and (2 2 0). It can be seen that ($\bar{D}_{LVP}$) is a little smaller than ($\bar{D}_{LFP}$), which is probably because of the suppression of the growth of crystalline LVP by excess carbon content.

The SEM images of the LFP/C and LVP/C samples are presented in Fig. 2a and b. As shown in Fig. 2a, a lot of nano/micron-sized LFP particles with granular shape are agglomerated to form large secondary particles, and they are well interconnected with the help

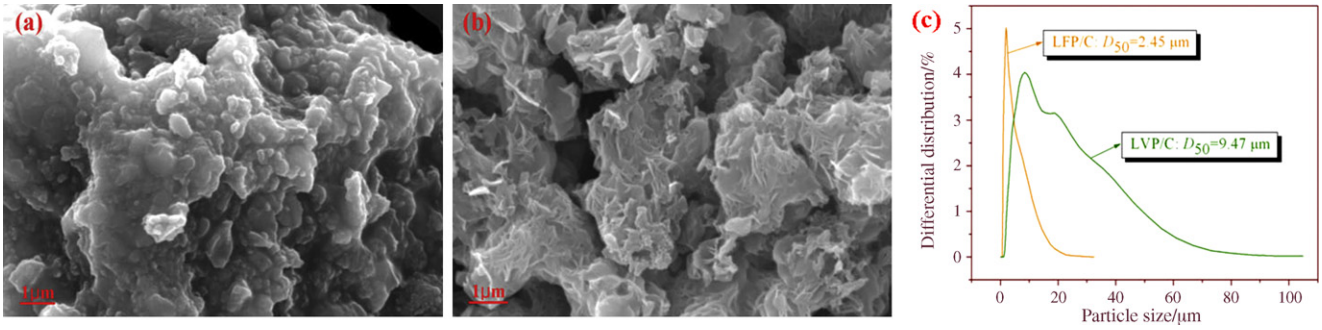

Fig. 2. SEM images of the LFP/C (a) and LVP/C (b) samples as well as their particle size distribution curves (c).

of the carbon network. The LVP/C sample (Fig. 2b) also displays an agglomerated morphology, which is formed by intertwining of a large number of flake shape microstructures and considered to be porous. Their particle size distribution curves are shown in Fig. 2c. The value of particle size at 50% cumulative population (D_{50}) for LFP/C and LVP/C samples is 2.45 and 9.47 μm, respectively. The narrower distribution curve of the LFP/C sample indicates the homogeneous particle size distribution of the powders. On the other hand, the LVP/C sample illustrates a broadened distribution curve due to the inhomogeneous particle size distribution caused by the intertwining of flake shape microstructures. In addition, we can find that D_{50}(LVP/C) is roughly comparable to its aggregate size, while, D_{50}(LFP/C) is much smaller than its aggregate size. Thus, it means that the LFP/C agglomerate can be easily dispersed, while LVP/C is relatively hard.

Fig. 3a displays the initial charge–discharge curves of the LFP/C sample at various low temperatures under a 0.3 C rate. At the temperature of 23 °C, the sample exhibits a flat and long voltage charge (3.5 V)/discharge (3.4 V) plateau, which indicates the two-phase

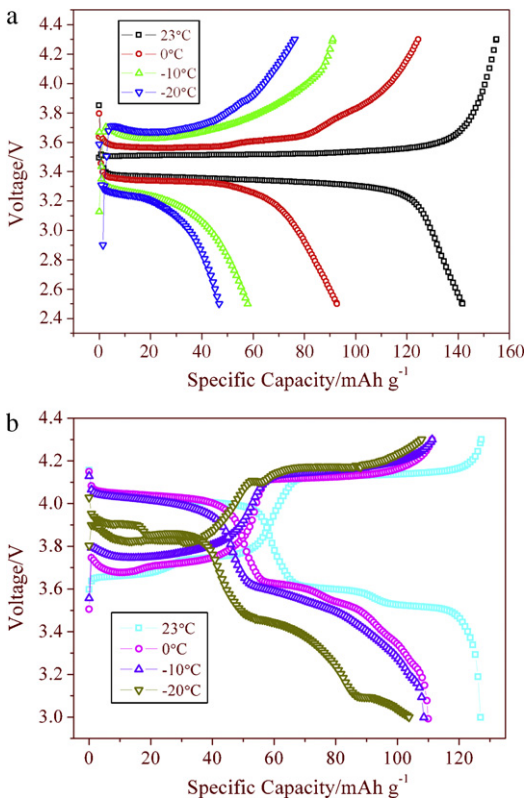

Fig. 3. The initial charge–discharge curves of the LFP/C (a) and LVP/C (b) samples at various low temperatures (23, 0, −10 and −20 °C) under a 0.3 C rate.

redox reaction process ($LiFePO_4 \Leftrightarrow FePO_4$) [2]. As the operation temperature decreases, the capacity decreases and the electrical polarization increases especially at −10 and −20 °C, as indicated by the voltage differences between the charge (increase) and discharge (decrease) plateaus. The initial discharge capacities for the LFP/C sample at temperatures of 23, 0, −10 and −20 °C are 141.8, 92.7, 57.9 and 46.7 mAh g^{-1} with the coulombic efficiency of 91.2%, 74.5%, 63.6% and 61.3%, respectively. Hence, at −20 °C, the cell only retains 32.9% of the discharge capacity obtained at 23 °C. The reduction of energy and power capability with decreasing temperature is probably attributed in literature to the decreased ionic conductivity of the electrolyte and solid electrolyte interface (SEI) film formed on the anode lithium metal surface, and limited diffusivity of lithium ions within the $LiFePO_4$ cathode, and the related polarization of the $LiFePO_4$ electrode, and substantially increased charge-transfer resistance on the electrolyte–electrode interfaces [27–30].

The initial charge–discharge curves of the LVP/C sample at various low temperatures are illustrated in Fig. 3b. As seen from the curves obtained at 23 °C, there are three charge flat plateaus (around 3.65, 3.73 and 4.15 V) and three discharge flat plateaus (around 3.51, 3.60 and 4.02 V), exhibiting the characteristic of two-phase behavior between the single phase of $Li_xV_2(PO_4)_3$ (x = 3.0, 2.5, 2.0 and 1.0). Similar to the case of the LFP/C sample, when the temperature decreases from 23 °C to −20 °C, both the capacity and operating discharge voltage of the LVP/C sample are also reduced. With lowering of the temperature, the initial discharge capacity of the LVP/C sample decreased to about 127.0 mAh g^{-1} (23 °C), 109.9 mAh g^{-1} (0 °C), 108.6 mAh g^{-1} (−10 °C) and 103.8 mAh g^{-1} (−20 °C) with corresponding coulombic efficiency of 99.8%, 98.8%, 97.6% and 96.2%, respectively. By comparing LFP/C and LVP/C, it can be found that not only the initial discharge capacity of LVP/C (103.8 mAh g^{-1}) at −20 °C but also the capacity proportion of −20 °C to 23 °C (81.7%) is much higher than those of LFP/C (46.7 mAh g^{-1}, 32.9%). Moreover, the coulombic efficiency of LVP/C can still reach 96.2% at −20 °C, while LFP/C owns only 61.3%, which indicates that, in a full lithium-ion cell, LVP/C is a more suitable cathode especially at −20 °C due to its less irreversible capacity loss.

Fig. 4 illustrates the cycling performance of the LFP/C and LVP/C samples at various low temperatures under a 0.3 C rate. For the LFP/C sample (Fig. 4a), it exhibits an excellent cycling capability with almost no capacity fading at various low temperatures. During cycles, the average discharge capacities at 23, 0, −10 and −20 °C are 144.2, 90.7, 55.5 and 45.4 mAh g^{-1}, respectively, which are very close to their initial discharge capacities. It should be noted that, with decreasing temperature, the capacity decreased rapidly, owning 62.9% (0 °C), 38.5% (−10 °C) and 31.5% (−20 °C) of the capacity obtained at 23 °C. In addition, with a careful observation of the cycling performance at −10 °C, it can be seen that the discharge capacity displays a small extent of periodic variation due to the temperature fluctuation (±4 °C) in the household refrig-

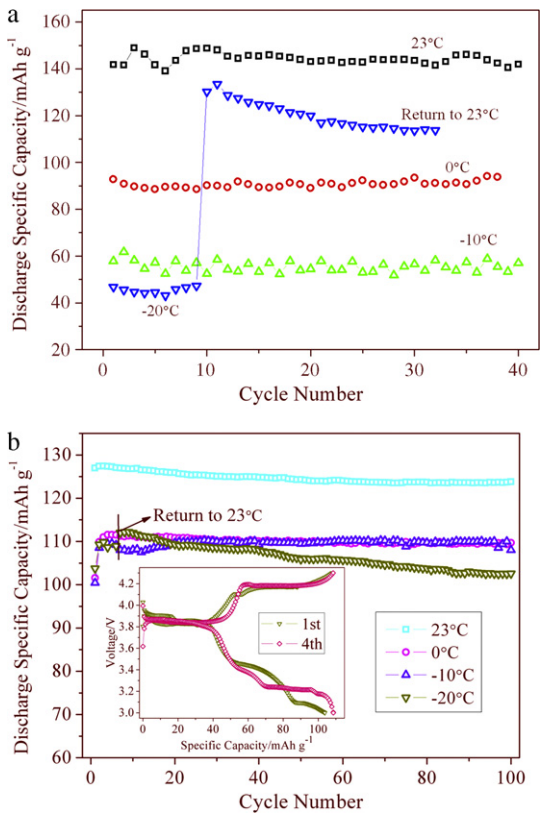

Fig. 4. The cycling performance of the LFP/C (a) and LVP/C (b) samples at various low temperatures under a 0.3 C rate. Inset of (b) is the 1st and 4th charge–discharge curves at −20 °C.

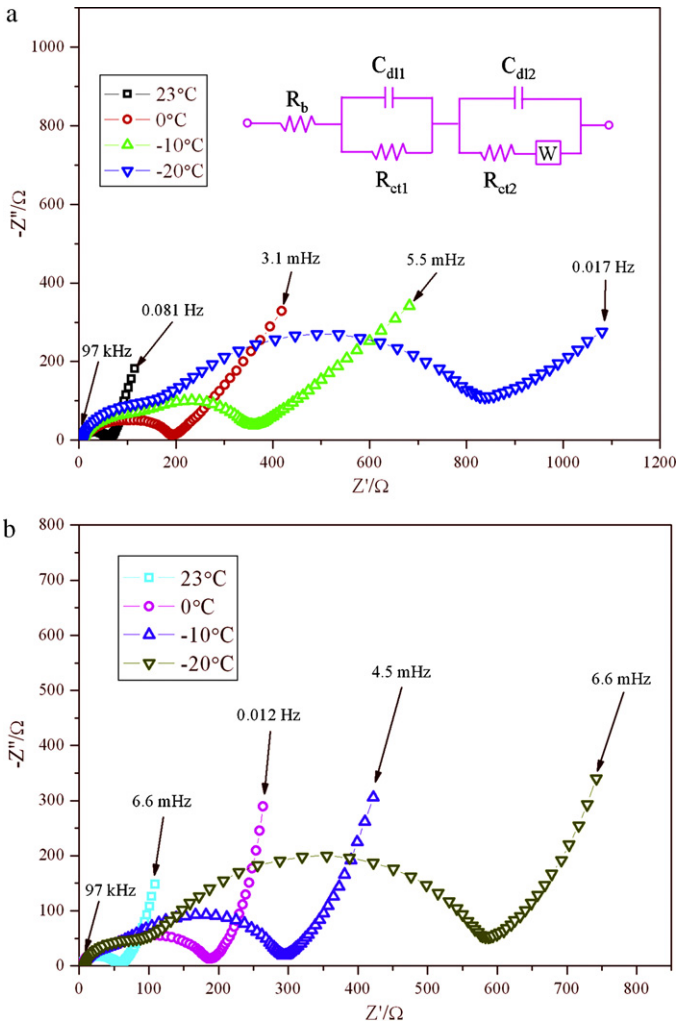

Fig. 5. Electrochemical impedance spectra of LFP/C (a) and LVP/C (b) cells measured at full charge state under various low temperatures. Inset of (a) analogs an equivalent circuit for the LFP/C or LVP/C half-cell.

erator, indicating that the LFP/C cathode is very sensitive to the low temperature varying (especially ≤−10 °C). In our experiments, when the cell completed the −20 °C cycling test, it was then heated back to 23 °C to continue its cycling test. We can find that the capacity can initially return to 130.2 mAh g^{-1} and shows a little fading during 23 cycles (capacity fading rate: 0.55% per cycle). As shown in Fig. 4b, for the LVP/C cell conducted at 23 °C, there is a slight capacity fading with a 100 cycles capacity retention of 97.5%. At −20 °C (inset of Fig. 4b), there still exist three stable discharge plateaus at around 3.85, 3.38 and 3.22 V that cause a relatively high discharge capacity and good cycling performance. On the other hand, the activation procedure is particularly needed at low temperatures, which displays an increasing discharge capacity during the initial several cycles. During cycles, the average discharge capacities are 124.7, 110.0, 109.5 and 108.1 mAh g^{-1} at 23, 0, −10 and −20 °C, respectively. It can be found that the discharge capacities at −20, −10 and 0 °C are very close, displaying 88.2% (0 °C), 87.8% (−10 °C) and 86.7% (−20 °C) of the capacity gained at 23 °C. In addition, similar to the LFP/C, when the LVP/C cell is recovered from −20 °C to 23 °C, it also illustrates an increasing capacity and a little capacity fading during 95 cycles (capacity fading rate: 0.97% per cycle). Overall, considering the low-temperature performance of the LFP/C and LVP/C cathodes (Figs. 3 and 4), we can find that the LVP cathode shows a superior low-temperature capability, especially at −10 and −20 °C.

To understand the origin of the superior low-temperature performance of the LVP/C to LFP/C, we firstly analyze their electrochemical impedance spectra (EIS) at various low temperatures, which were measured at the 6th full charge state. Fig. 5 presents EIS of LFP/C and LVP/C cells at various low temperatures. From Fig. 5, it is apparently seen that the impedance spectrum is composed of two partially overlapped semicircles at high and medium frequency regions, and a straight slopping line at low frequency regions. Such a pattern in the impedance spectra can be simply explained by an equivalent circuit shown in the inset of Fig. 5a. The R_b represents bulk resistance of the cell, which reflects the overall ohmic resistance of the electrolyte, and electrodes; R_{ct1} and C_{dl1} are the charge-transfer resistance and its related double-layer capacitance between the electrolyte and lithium metal anode, which correspond to the semicircle at high frequencies; R_{ct2} and C_{dl2} are the charge-transfer resistance and its related double-layer capacitance between the electrolyte and cathode, corresponding to the semicircle at medium frequencies; W is the Warburg impedance related to the diffusion of lithium ions in the electrode, which is indicated by a straight slopping line at low frequencies. The combination of R_{ct2} and W is called Faradic impedance, which reflects the kinetics of the cell reactions. High R_{ct2} generally corresponds to a slow kinetics of the Faradic reaction. As shown in Fig. 5, it is apparently seen that R_{ct2} of LFP/C and LVP/C samples increased rapidly with the temperature falling, which adequately explains why their electrochemical performance decreases as the temperature decreased. Moreover, by comparing R_{ct2} values at various low temperatures, it can be found that the R_{ct2} values of the LFP/C cell are all larger than those of the LVP/C cell, e.g. at −20 °C, LFP/C: 781 Ω and LVP/C: 503 Ω, which is a reason that the low-temperature performance of the LVP/C is superior to the LFP/C.

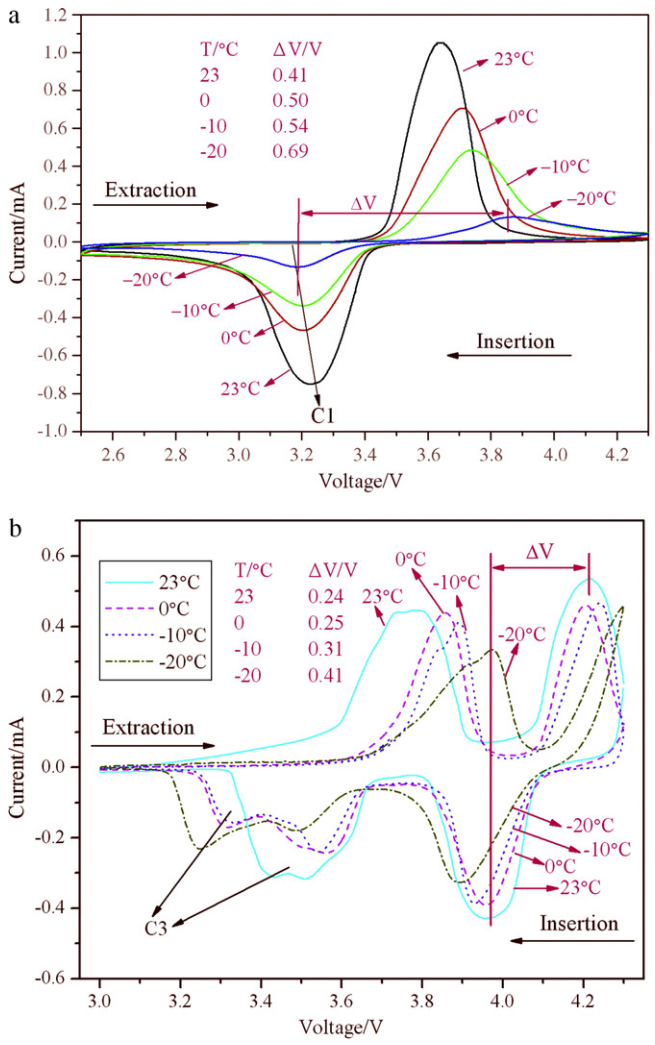

Fig. 6. The CV curves of the LFP/C (a) and LVP/C (b) samples in the second cycle at various low temperatures using a scanning rate of 0.1 mV s^{-1}.

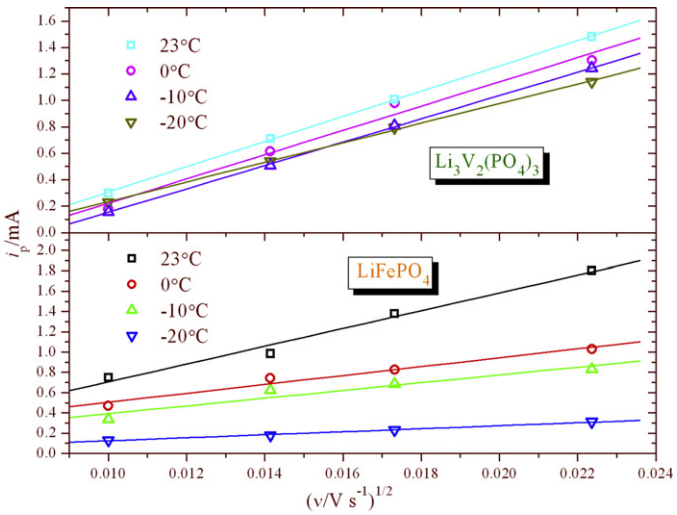

Fig. 7. The relationship of the cathodic C1 and C3 peak current (i_p) and the square root of scan rate ($v^{1/2}$).

Fig. 6 illustrates the cyclic voltammogram (CV) curves of the LFP/C and LVP/C samples in the second cycle at various low temperatures using a scanning rate of 0.1 mV s^{-1}, in which the voltage difference (ΔV) between the anodic and cathodic peaks can be easily measured. As shown in Fig. 6a, a pair of redox peaks appears in the CV curves of the LFP/C sample, which corresponds to the two-phase charge/discharge reaction of the Fe^{2+}/Fe^{3+} redox couple. For simplicity, we always compare the ΔV value as a parameter to estimate the passivation or polarization levels. The ΔV values for LFP/C at various low temperatures of 23, 0, −10 and −20 °C are 0.41, 0.50, 0.54 and 0.69 V, respectively, which indicates that the polarization increases with decreasing temperature during the redox process. It is mainly because of a decrease in the ionic conductivity of electrolyte as well as a slowdown of the cell electrochemical reactions. For the LVP/C sample (Fig. 6b), there are three oxidation peaks and three corresponding reduction peaks, which are associated with V^{3+}/V^{4+} redox couple. According to ΔV values, similar to LFP/C, the polarization of LVP/C cells also increases as the temperature decreases. For example, ΔV values for the peak associated with the second lithium ion extraction/intercalation at temperatures of 23, 0, −10 and −20 °C are 0.24, 0.25, 0.31 and 0.41 V, respectively, which are lower than those of LFP/C sample, implying that the polarization of LFP/C cells is larger than LVP/C cells.

To further investigate the electrode kinetics, the apparent chemical diffusion coefficient of lithium ions ($D^{app}_{Li^+}$) in LFP and LVP for Li^+ full intercalation at various low temperatures is estimated by a previously reported CV method [31,32]. The cathodic C1 (LFP) and C3 (LVP) peaks as marked in Fig. 6 respectively correspond to one lithium intercalation into $FePO_4$ and 0.5 lithium intercalation into $Li_{2.5}V_2(PO_4)_3$ to form full intercalation state of $LiFePO_4$ and $Li_3V_2(PO_4)_3$, which are used to calculate the $D^{app}_{Li^+}$ of LFP and LVP. The CV curves of LFP/C and LVP/C electrodes at temperatures of 23, 0, −10 and −20 °C under the scan rates of 0.1, 0.2, 0.3 and 0.5 mV s^{-1} were conducted, which are not shown here. As shown in Fig. 7, it is found that the cathodic C1 and C3 peak current (i_p) has a linear relationship with the square root of scan rate ($v^{1/2}$), which is typical of the equilibrium behavior of an intercalation type electrode. If the charge transfer at the interface is fast enough and the rate-limiting step is the lithium diffusion in electrode, the relationship of the peak current and the CV sweep rate is:

$$i_p = \left(2.69 \times 10^5\right)\ n^{3/2} S D^{1/2}_{Li^+} C^*_{Li} v^{1/2} \quad (1)$$

where i_p is the peak current (A), n is the charge-transfer number, S is the contact area between electrode and electrolyte (here the geometric area of electrode, 1.54 cm^2, is used for simplicity), C^*_{Li} is the concentration of lithium ions in the cathode, and v is the potential scan rate (V s^{-1}). Based on Eq. (1) and the slope of i_p vs. $v^{1/2}$ plots in Fig. 7, the $D^{app}_{Li^+}$ values of LFP and LVP at various low temperatures are determined and the results are shown in Table 1. It can be found that the $D^{app}_{Li^+}$ values of LFP are in a magnitude of 10^{-11} cm^2 s^{-1}, which are an order lower than those of LVP. In addi-

Table 1
The apparent chemical diffusion coefficient of lithium ions of LFP and LVP at various low temperatures.

	T, °C			
	23	0	−10	−20
D^{app}_{Li+}(LFP)/ × 10^{-11} cm^2 S^{-1}	8.63	2.16	1.64	0.25
D^{app}_{Li+}(LVP)/ × 10^{-10} cm^2 S^{-1}	8.66	8.02	7.41	5.22

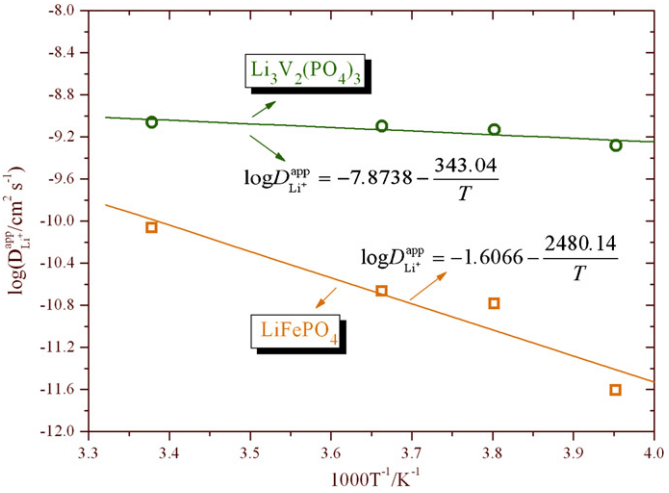

Fig. 8. Arrhenius plots of the apparent chemical diffusion coefficient of lithium ions of the LFP and LVP.

tion, with the temperature decreasing, no matter the LFP or the LVP, the $D_{Li^+}^{app}$ all decrease. However, the $D_{Li^+}^{app}$ decreasing rate of LFP as the temperature is much larger than that of LVP. Thus, it can be concluded that the LFP electrode kinetics is more sluggish than LVP, especially at low temperature of −20 °C.

To see more clearly the temperature effect on $D_{Li^+}^{app}$, the logarithmic $D_{Li^+}^{app}$ was plotted against the inverse of temperature (Fig. 8), and the resultant plots follow the conventional Arrhenius equation:

$$D_{Li^+}^{app} = D_0 \exp\left(\frac{-E_a}{RT}\right) \quad (2)$$

where D_0 is the pre-exponential factor (a temperature-independent coefficient), E_a is the activation energy, R is the gas constant, T is the absolute temperature. On the basis of Eq. (2), the activation energies ($E_a = -Rk \ln 10$, k is the slope of the fitting line shown in Fig. 8) of LFP and LVP are calculated to be 47.48 and 6.57 kJ mol^{-1}, respectively. The activation energy of LVP is about one seventh that of LFP, indicating an easier diffusion for lithium extraction/intercalation.

4. Conclusion

The electrochemical tests illustrate that the low-temperature performance of LVP/C is much better than that of LFP/C in a general electrolyte (1.0 M $LiPF_6$/EC + DMC (1:1 w/w)). At −20 °C, the LFP/C sample has only a stable reversible discharge capacity of 45.4 mAh g^{-1} under 0.3 C rate, which owns 31.5% of the capacity obtained at 23 °C. For the LVP/C sample, it delivers a high stable reversible discharge capacity of 108.1 mAh g^{-1} at −20 °C under 0.3 C rate, owning 86.7% of the capacity gained at 23 °C. The EIS measurement shows that the charge-transfer resistance R_{ct2} values of LFP/C at various low temperatures are all greater than those of LVP/C. Moreover, in CV curves, the ΔV values of LFP/C at various low temperatures are all larger than those of LVP/C, implying that the cell polarization of LVP/C is relatively low. Also, the $D_{Li^+}^{app}$ measurement shows that not only $D_{Li^+}^{app}$ values of LFP at various low temperatures are lower than those of LVP, but also the $D_{Li^+}^{app}$ decreasing rate of LFP with the temperature is much larger, meaning that the LFP electrode kinetics is more sluggish. The activation energies of LFP and LVP are calculated to be 47.48 and 6.57 kJ mol^{-1}, indicating that the extraction/intercalation of Li^+ in LVP is much easier than in LFP.

Acknowledgments

This study was supported by National Science Foundation of China (grant nos. 20971117 and 10979049) and Education Department of Anhui Province (grant no. KJ2009A142). We are also grateful to the Solar Energy Operation Plan of Academia Sinica.

References

[1] B. Scrosati, Nature 373 (1995) 557.
[2] A.K. Padhi, K.S. Nanjundaswamy, J.B. Goodenough, J. Electrochem. Soc. 144 (1997) 1188.
[3] A. Yamada, S.C. Chung, K. Hinokuna, J. Electrochem. Soc. 148 (2001) A224.
[4] N.N. Bramnik, K. Nikolowski, C. Baehtz, K.G. Bramnik, H. Ehrenberg, Chem. Mater. 19 (2007) 908.
[5] W.F. Howard, R.M. Spotnitz, J. Power Sources 165 (2007) 887.
[6] H. Huang, S.C. Yin, T. Kerr, N. Taylor, L.F. Nazar, Adv. Mater. 14 (2002) 1525.
[7] F. Zhou, M. Cococcioni, K. Kang, G. Ceder, Electrochem. Commun. 6 (2004) 1144.
[8] A. Aatiq, M. Menetrier, L. Croguennec, E. Suardc, C. Delmasb, J. Mater. Chem. 12 (2002) 2971.
[9] Z. Chen, J.R. Dahn, J. Electrochem. Soc. 149 (2002) A1184.
[10] J. Shim, K.A. Striebel, J. Power Sources 119–121 (2003) 955.
[11] M.Y. Saidi, J. Barker, H. Huang, J.L. Swoyer, G. Adamson, J. Power Sources 119–121 (2003) 266.
[12] S.C. Yin, H. Grondey, P. Strobel, M. Anne, L.F. Nazar, J. Am. Chem. Soc. 125 (2003) 10402.
[13] S.C. Yin, H. Grondey, P. Strobel, H. Huang, L.F. Nazar, J. Am. Chem. Soc. 125 (2003) 326.
[14] S.C. Yin, P.S. Strobel, H. Grondey, L.F. Nazar, Chem. Mater. 16 (2004) 1456.
[15] S.Y. Chung, J.T. Bloking, Y.M. Chiang, Nat. Mater. 1 (2002) 123.
[16] H. Liu, Q. Cao, L.J. Fu, C. Li, Y.P. Wu, H.Q. Wu, Electrochem. Commun. 8 (2006) 1553.
[17] D. Wang, H. Li, S. Shi, X. Huang, L. Chen, Electrochim. Acta 50 (2005) 2955.
[18] P. Fu, Y.M. Zhao, Y.Z. Dong, X.N. An, G.P. Shen, J. Power Sources 162 (2006) 651.
[19] X.H. Rui, C. Li, C.H. Chen, Electrochim. Acta 54 (2009) 3374.
[20] I. Belharouak, C. Johnson, K. Amine, Electrochem. Commun. 7 (2005) 983.
[21] Q.Q. Chen, J.M. Wang, Z. Tang, W.C. He, H.B. Shao, J.Q. Zhang, Electrochim. Acta 52 (2007) 5251.
[22] X.Z. Liao, Y.S. He, Z.F. Ma, X.M. Zhang, L. Wang, J. Power Sources 174 (2007) 720.
[23] H.H. Chang, C.C. Chang, C.Y. Su, H.C. Wu, M.H. Yang, N.L. Wu, J. Power Sources 185 (2008) 466.
[24] X.H. Rui, C. Li, J. Liu, T. Cheng, C.H. Chen, Electrochim. Acta 55 (2010) 6761.
[25] H.C. Shin, W.I. Cho, H. Jang, J. Power Sources 159 (2006) 1383.
[26] Y.Z. Li, Z. Zhou, X.P. Gao, J. Yan, Electrochim. Acta 52 (2007) 4922.
[27] S.S. Zhang, K. Xu, T.R. Jow, J. Power Sources 115 (2003) 137.
[28] S.S. Zhang, K. Xu, T.R. Jow, Electrochim. Acta 49 (2004) 1057.
[29] B.V. Ratnakumar, M.C. Smart, S. Surampudi, J. Power Sources 97–98 (2001) 137.
[30] C.S. Wang, A.J. Appleby, F.E. Little, J. Electrochem. Soc. 149 (2002) A754.
[31] X.H. Rui, N. Ding, J. Liu, C. Li, C.H. Chen, Electrochim. Acta 55 (2010) 2384.
[32] K. Wang, R. Cai, T. Yuan, X. Yu, R. Ran, Z.P. Shao, Electrochim. Acta 54 (2009) 2861.